CHAPTER 2

ZERO FIELD SPLITTING IN Mn (III) COMPLEXES: A COMPARATIVE STUDY OF DFT BASED COUPLED-PERTURBED AND PEDERSON-KHANNA APPROACHES

INTRODUCTION

Zero-field spitting (ZFS) and g-tensor are the two EPR parameters which can characterize the magnitude and anisotropy of a molecule in a given electronic state. Manganese monomers [1,2] and clusters [3,4] are inextricably associated with biological reactions as enzymes, [5,6] and oxidation of organic substances, [7,8] as catalysts. Mn(III) ions are open-shell transition metal systems and hence they are characterized owing to their paramagnetism. Therefore, they are amenable to EPR spectroscopy. We have focused our attention to the investigation of the magnetic properties of Mn(III) complexes since in recent times molecular superparamagnets such as single molecule magnets (SMMs) [9,10] and single-chain magnets (SCMs) [11,12,13], where uniaxial anisotropy originates from metal ions, have undergone remarkable breakthrough. It has been found that Mn(III) is the most promising contender among other transition metals for producing large negative axial D-tensor values that satisfy SMM behaviors [14]. As required in SMMs, Mn(III) is a discrete molecular species which can retain a magnetic moment after removing an applied magnetic field. There are reports where axial zero-field splitting parameters D-tensors in Mn(III) complexes are calculated theoretically [15].

In the present work we have carried out DFT studies on a set of experimentally well-characterized 5- and 6-coordinated Mn(III) high-spin complexes. Their experimental data are derived from various references. The complexes are: Mn(terpy)F_3 (**1**), Mn(terpy)Cl_3 (**2**), Mn(tpp)Cl (**3**), Mn(tpp)(py)Cl (**4**), Mn(salen)SCN (**5**), Mn(salen)Br (**6**) and Mn(pterpy)F_3 (**7**) where terpy=2,2′:6″,2″-terpyridine; tpp=5,10,15,20-tetraphenylporphyrin; salen=*N*,*N*″-ethylene-bis(salicylideneiminate) and pterpy=4′-phenyl-,2′:6′,2″-terpyridine. Mn(III) ion possessing a d^4 configuration is known to exhibit Jahn-Teller distortion. It has an integer spin ground state S=2 and the ground term for this high-spin Mn(III) ion is ^5D which splits into $^5T_{2g}$ and ^5E_g terms in presence of an octahedral field. Further the ^5E_g ground term splits into $^5A_{1g}$ or $^5B_{1g}$ under the effect

of non-cubic symmetry or Jahn–Teller distortion to generate D_{4h} symmetry. Subsequently the spin degeneracy of the ground state is further removed by spin-orbit coupling giving rise to zero-filed splitting [16]. Therefore, high-spin d^4 configuration of Mn(III) splits into 5 sub-levels as $M_S=0, \pm1, \pm2$. It is well-established that the large Jahn-Teller distortion that is characteristic of d^4 Mn(III) complexes, being in high oxidation state, results in axial elongation with negative ZFS value [17]. This is illustrated in Figure 2.1.

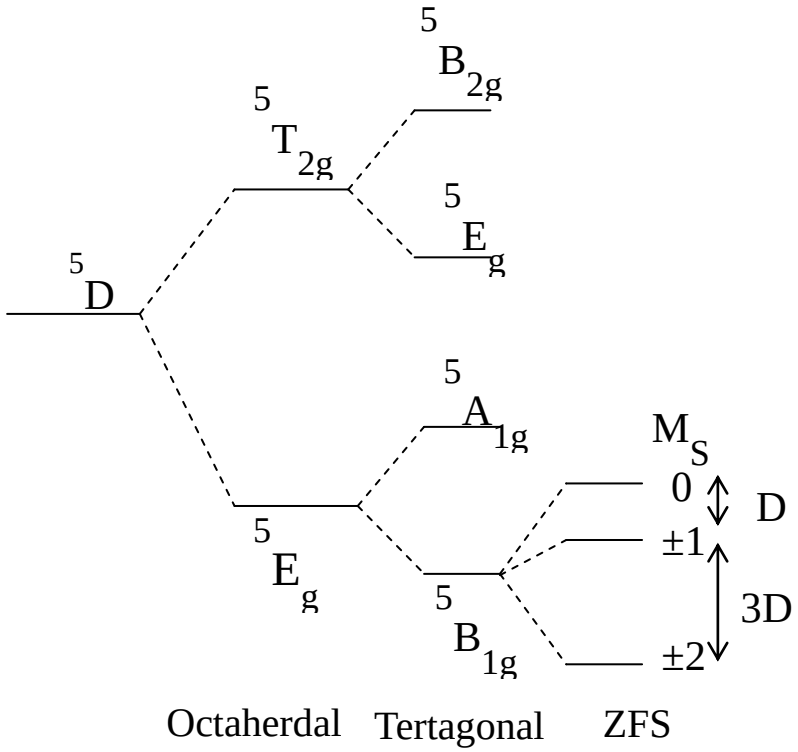

Figure 2.1: Splitting of the ^5D term (d^4) by octahedral and tetragonal (axially elongating) fields and by second-order spin-orbit coupling (zero-field splitting).

The two most remarkable parameters in magnetic studies are ZFS or D-tensor and electronic g-tensor. The information they provide is monotonous in determining relations between electronic structure and chemical properties. Much of the contribution in calculation of g-tensor is made by the first-principle calculations [18-21]. Traditional *ab initio* calculations of g-tensor proved to be expensive since they require large basis sets and sophisticated treatment of the electron correlation, whereas DFT permits for an inexpensive treatment of the electron correlation and successfully study other properties of the transition metal complexes, [22] thus making it a tool for

choice of such calculations. Apart from g-tensor, systems possessing spin $>\frac{1}{2}$ are characterized by ZFS parameter or D-tensor [23]. In organic radical the D-tensor tends to be dominated by the direct dipolar spin-spin coupling (SS), and on the other hand, spin-orbit coupling (SOC) dominates in case of open-shell transition metal complexes of relevance in molecular magnetism [24]. In transition metal complexes, D-tensor relies largely on ligand field theory [25].

We have performed g-tensor and D-tensor DFT calculations on the test series and a comparative study between the experimental and the theoretical values using different methodologies for choosing the best approach which gives better agreement with the experimental values. It must be mentioned here that we have studied the magnetic properties of the optimized structures even when the experimental structures may be available because the well-defined points on the potential energy surfaces are fairly represented by the theoretically optimized structures rather than the experimentally derived ones. Also such geometries are free from inaccuracies pertaining to the experimental structures.

2.1 Theory

Electronic g-tensors of molecules provide insight in electronic interactions on the unpaired electron of the molecules. But experimentally derived g-tensor values are not reliable when it comes to the extraction of information regarding electronic interactions. As such, theoretical calculations of g-tensor are beneficial for interpretation of experimental results since they allow for the establishment of relationships between the g-tensor and the electronic structure of the concerned molecule. The decomposed form of electronic g-tensor is:

$$\boldsymbol{g} = \boldsymbol{g}_e 1 + \Delta \boldsymbol{g}$$

where '$\boldsymbol{g}$' stands for electronic g-tensor, $\boldsymbol{g}_e$ is the g-factor for free electron (2.0023) and $\Delta \boldsymbol{g}$ is the g-tensor shift. The g-shift is unique to every molecule since it is a characteristic quantity of the local environment of the unpaired electrons in the molecule.

Mathematically, g-tensor is defined as the second-derivative of the electronic energy E of a many-body system with respect to the applied magnetic field denoted by **B** and the total electron spin **S**:

$$\boldsymbol{g} = \frac{1}{\mu_B} \frac{\partial^2 E}{\partial \boldsymbol{B} \partial \boldsymbol{S}}\bigg|_{B=0, S=0}$$

Therefore, the corresponding g-shift, Δg can be analogously written as:

$$\Delta \boldsymbol{g} = \frac{1}{\mu_B} \frac{\partial^2 E}{\partial \boldsymbol{B} \partial \boldsymbol{S}}\bigg|_{B=0, S=0} - \boldsymbol{g_e} 1$$

where μ_B corresponds to the Bohr magneton.

The approximation for the g-shift, $\Delta \boldsymbol{g}$ has been extensively pursued on the basis of Breit-Pauli Hamiltonian [14,18,26]. It treats relativistic corrections, magnetic field dependent terms and more importantly spin as perturbations. This approximation is employed for both non-relativistic *ab initio* and DFT methods for calculation of g-tensor based on perturbation theory [14,16, 27 , 28]. Treating $\Delta \boldsymbol{g}$, up to the level of second-order perturbation theory, the $\Delta \boldsymbol{g}$ consists of the relevant Breit-Pauli terms:

$$\Delta \boldsymbol{g} = \Delta \boldsymbol{g_{RMC}} + \Delta \boldsymbol{g_{GC}} + \Delta \boldsymbol{g_{SO/OZ}}$$

where the first term corresponds to mass-correction term, second term to one-electron gauge-correction to the electronic Zeeman effect while the last term denotes one-electron spin-orbit corrections coupled with the orbital Zeeman effect.

The d^4 system of Mn(III) is characterized by 5 magnetic sublevels, ± 2, ± 1 and 0. Within a non-relativistic or scalar relativistic treatment, these levels remain energetically degenerate. But when Zeeman effect, spin-orbit coupling and dipolar spin-spin coupling are included their degeneracy is lifted [29,30]. The effective spin Hamiltonian, H_{spin} of these interactions, excluding nuclear spin and exchange interactions, is written as:

$$H_{spin} = H_{Ze} + H_{ZFS} = \mu_B \vec{B}_g \vec{S} + \vec{S} D \vec{S}$$

where, $\vec{B}$ stands for magnetic flux density, $\vec{S}$ denotes effective spin operator and g and D are the g-tensor and D-tensor or zero-field spitting (ZFS) tensor, respectively. The ZFS describes the removal of the state degeneracy for systems with S>1/2 in absence of magnetic field. By choosing a coordinate system that diagonalizes D, we can express H_{ZFS} as:

$$H_{ZFS} = D\left[S_z^2 - \tfrac{1}{3}S(S+1)\right] + E\left(S_x^2 - S_y^2\right),$$

$$D = D_{zz} - \frac{1}{2}\left(D_{xx} - D_{yy}\right)$$

Here, D and E are axial and rhombic ZFSs. D and E are such that they are in a coordinate system that satisfies the Blumberg convention, [31] which is commonly used in transition metal complexes:

$$|D_{zz}| > |D_{yy}| > |D_{xx}|$$

and this convention yields $0 \leq \frac{E}{D} \leq \frac{1}{3}$. For axially symmetric system the parameter E vanishes.

ZFS or D-tensor is known to be constituted by two parameters and the relative importance of the following two distinct contributions to the ZFS is well predicted:[20,26,32] (i) Interaction of the classical dipole magnetic moments of pairs of electrons give rise to first-order term of direct dipolar spin-spin interaction between pairs of electrons and this contribution is denoted by D_{ss}, (ii) spin-orbit coupling (SOC) give rise to a second-order term that introduces some angular momentum into the ground state (which was orbitally nondegenerate) and which is being picked up by the spin of a second electron, D_{SOC}. The calculation of D_{ss} involves only the ground state wave function whereas same-spin and spin-flip excited states interaction with ground state contributes to D_{SOC}.

According to McWeeny and Mizuno formula [33] the spin-spin part of the D-tensor can be estimated on the basis of the ground state Slater determinant, as follows:

$$D_{K,L} = -\frac{g_e^2}{16}\frac{\alpha^2}{S(2S-1)} \times$$

$$\sum_{\mu\nu\kappa\tau} \left\{ P_{\mu\nu}^{\alpha-\beta} P_{\kappa\tau}^{\alpha-\beta} - P_{\mu\kappa}^{\alpha-\beta} P_{\nu\tau}^{\alpha-\beta} \right\} \left\langle \mu\nu \middle| r_{12}^{-5} \{ 3 r_{12,K} r_{12,L} - \delta_{K,L} r_{12}^2 \} \middle| \kappa\tau \right\rangle$$

where $P^{\alpha-\beta} = P^{\alpha} - P^{\beta}$ is the spin density matrix with $P_{\mu\nu}^{\sigma} = \sum_{p\sigma} c_{\mu p}^{\sigma} c_{\nu p}^{\sigma}$ and $c^{\sigma}$is the MO coefficient matrix for spin σ; α is the fine structure constant (~ 1/137 in atomic units).

Detailed calibrated work by Sinnecker and Neese [25] revealed that the spin-unrestricted DFT calculation gives somewhat erratic values which are corrected by open-shell spin restricted DFT. Therefore, the 'UNO' treatment allows the calculation of the D_{ss} term with a restricted spin-density obtained from the singly-occupied unrestricted natural orbitals [34]. We have considered SS-UNO for D_{ss} calculation. UNO is also advantageous because it can be conveniently diagonalized together with the contributions obtained from any other method used for calculation of SOC (eg., SOC-PK or SOC-CP). The SOC operator will then clutch to the functional and DFT method will become more consistent with the finding of the result.

For the calculation of D_{SOC} two approximations were developed: PK (Pederson and Khanna) method and a linear response method referred to as couple-perturbed SOC (CP-SOC) approach. As previously found the combination of CP approach for the SOC part of the D-tensor and the spin-unrestricted natural orbital (UNO) variant for the calculation of the spin-spin coupling of the D-tensor yields D values closer to the experimentally derived values [20,28,35-39]. Frank Neese forwarded that CP-SOC approach along with a hybrid DFT functional leads to a slope of the correlation line (plot of experimental vs. calculated D-values) that is unity. More importantly previously published benchmark calculations on a mononuclear Mn(II) and Mn(III) complexes [20,35,35,40] used this method. Comparative study between PK and CP revealed that the CP-SOC method is more successful mainly due to the revised pre-factors for the spin-flip terms. In this paper we have evaluated the D_{SOC} using both the CP and the PK method and have made a comparative study between the two.

2.2 Computational Details

The optimizations as well as the magnetic parameter, g-tensor and D-tensor calculations were done in the ORCA program package [34,41,42]. The BP [43,44] functional, the Karlsruhe polarized triple-zeta valence basis set (TZVP) [45] and the auxiliary def2-TZV/J [46] basis set for resolution of identity (RI) approximation were employed for the geometry optimizations. Optimizations were performed in the high-spin state. Additionally denser integration grids (Grid4 in ORCA convention) and *TightSCF* convergence criteria were used. The SOC operator is represented by an effective one-electron with the spin-orbit mean-field (SOMF) method [47].

2.3 Results and discussion

The optimized structures of the complexes are shown in Figure 2.2 and they are numbered as mentioned earlier and Table 2.1 with the summary of experimental data.

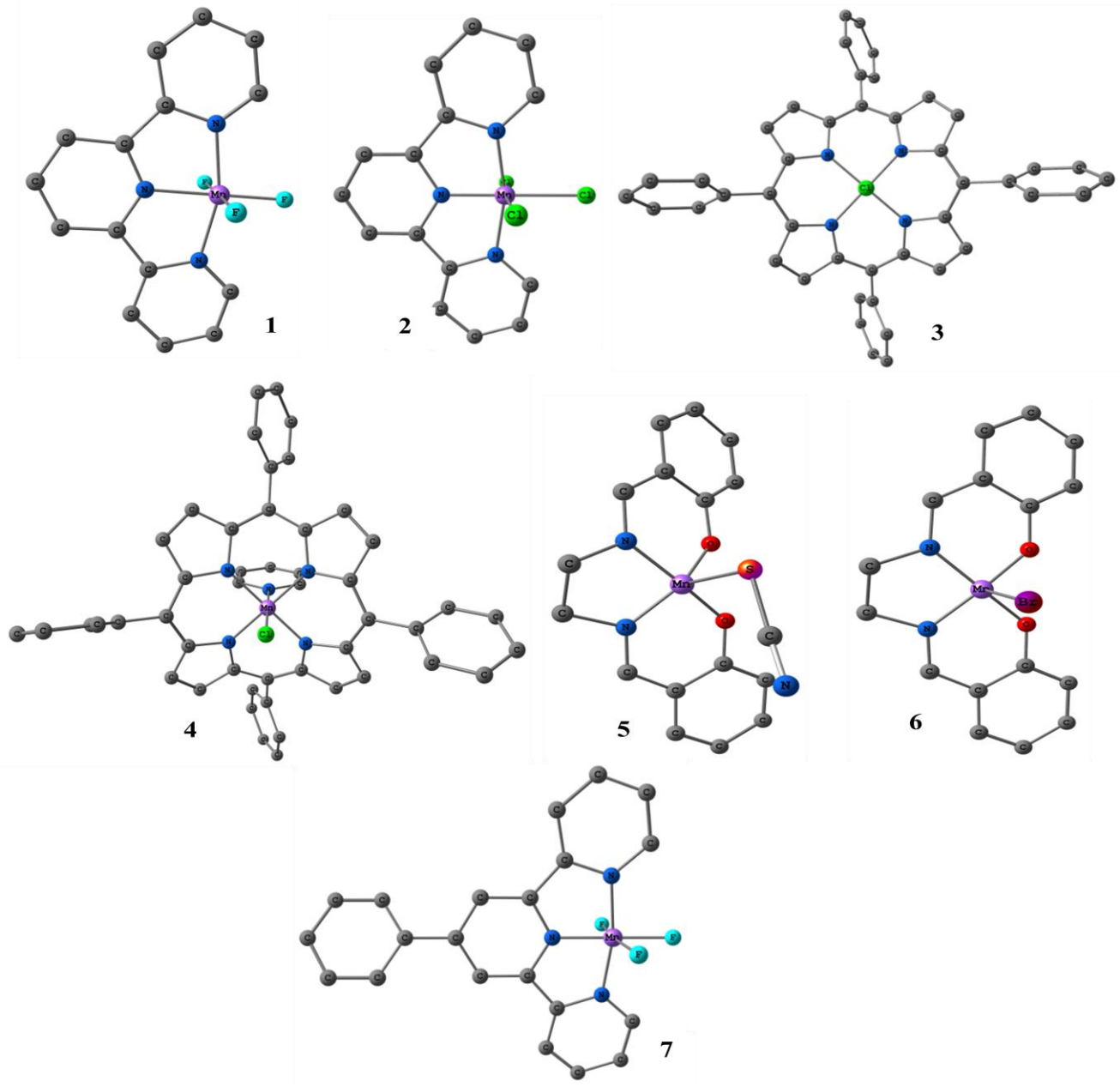

Figure 2.2: Optimized molecular structures of Mn(III) complexes studied in this work. Hydrogen atoms are omitted for clarity.

Table 2.1: Experimental data of the Mn(III) complexes with references

Sl. No.	Complexes	Coordination sphere	D_{exp} (cm^{-1})	Ref.
1	[Mn(terpy)F_3]	N3F3	-3.83	48
2	[Mn(terpy)Cl_3]	N3Cl3	-3.46	49
3	[Mn(tpp)Cl]	N4Cl	-2.29	50
4	[Mn(tpp)(py)Cl]	N5Cl	-3.50	51
5	[Mn(salen)SCN]	N2O2S	-3.80	52
6	[Mn(salen)Br]	N2O2Br	-1.00	52
7	[Mn(pterpy)Cl_3]	N3Cl3	-3.53	49

The bond lengths of Mn and the other atoms as in N, F Cl, etc. are listed in Table 2.2.

Table 2.2. Bond lengths of Mn atom with ligand atoms

Complexes	$Mn(terpy)F_3$	$Mn(terpy)Cl_3$	Mn(tpp)Cl	Mn(tpp)(py)Cl	Mn(salen)SCN	Mn(salen)Br	$Mn(pterpy)Cl_3$
d(Mn–N1)/Å	1.988	1.859	1.847	1.862	1.790	1.754	1.860
d(Mn–N2)/Å	1.962	1.746	1.849	1.862	1.742	1.749	1.838
d(Mn–N3)/Å	1.988	1.861	1.845	1.861			1.862
d(Mn–N4)/Å	–	–	1.846	1.862			
d(Mn–N5)/Å	–	–	–	1.867			
d(Mn–F1)/Å	1.807						
d(Mn–F2)/Å	1.795						
d(Mn–F3)/Å	1.807						
d(Mn–Cl1)/Å		2.164	2.187	2.157			2.167
d(Mn–Cl2)/Å		2.162					2.164
d(Mn–Cl3)/Å		2.162					2.164
d(Mn–O1)/Å					1.773	1.754	
d(Mn–O2)/Å					1.738	1.749	
d(Mn–Br)/Å						2.395	
d(Mn–S)/Å					2.174		

By performing single point calculations on the optimized structures we obtain g-values close to 2. This implies the anisotropy of Zeeman interaction being very small. However, the isotropic g-values show small deviations from the free g-values. Also the g_x, g_y and g_z values range from 1.9 to 2.0 and this confirms lack of anisotropy in the high-spin Mn(III) complexes. Table 2.3 summarizes all the g-values in the x, y and z coordinates as well as the isotropic g-tensors and also the g-shift values and the corresponding g-shift isotropic values.

Table 2.3: Calculated g-tensor and g-shift values

Sl. No.	Complexes	g_{tot}			g_{iso}	Δg_{tot}			Δg_{iso}
1	[Mn(terpy)F_3]	1.998	1.999	1.999	1.999	-0.0040	-0.003	-0.003	-0.003
2	[Mn(terpy)Cl_3]	2.002	2.005	2.007	2.005	0.0001	0.003	0.005	0.002
3	[Mn(tpp)Cl]	1.998	2.005	2.005	2.003	-0.0041	0.003	0.0035	0.001
4	[Mn(tpp)(py)Cl]	1.997	2.002	2.006	2.002	-0.0051	-0.000	0.0035	-0.001
5	[Mn(salen)SCN]	2.008	2.009	2.018	2.012	0.0061	0.007	0.0165	0.001
6	[Mn(salen)Br]	1.998	1.998	1.999	1.999	-0.0014	-0.003	-0.003	-0.003
7	[Mn(pterpy)Cl_3]	1.999	2.002	2.003	2.002	-0.002	-0.001	0.001	-0.001

From the decomposed $\Delta\mathbf{g}$ values we observe that the gauge-correction term, $\Delta\mathbf{g}_{\mathrm{GC}}$ and the second-order spin-orbit/orbital Zeeman cross term $\Delta\mathbf{g}_{SO/OZ}$ contribute negligibly ($\Delta\mathbf{g}_{\mathrm{GC}}$ contributes ~0.013–0.015% and $\Delta\mathbf{g}_{SO/OZ}$ contributes ~0.1–0.2%) to the g-tensor shift. It is known that the term $\Delta\mathbf{g}_{\mathrm{GC}}$ contributes appreciably only in the absence of spin-orbit contributions. Conversely it implies that there is significant spin-orbit contribution in these high-spin Mn(III) complexes. Therefore, contribution from $\Delta\mathbf{g}_{\mathrm{GC}}$ and $\Delta\mathbf{g}_{SO/OZ}$ can be neglected without compromising the accuracy. The most dominating term is, therefore, the relativistic mass-correction term, $\Delta\mathbf{g}_{\mathrm{RMC}}$.

The corresponding D-values calculated for the complexes are summarized in Table 2.4.

Table 2.4: Experimental and calculated D-tensor values

Sl. No.	Complexes	D_{Exp}	D_{Tot}		E/D	
			CP-SOC	PK-SOC	CP-SOC	PK-SOC
1	[Mn(terpy)F_3]	-3.83	-3.44	-2.82	0.18	0.08
2	[Mn(terpy)Cl_3]	-3.46	-2.98	-2.65	0.25	0.10
3	[Mn(tpp)Cl]	-2.29	-1.83	-1.78	0.02	0.01
4	[Mn(tpp)(py)Cl]	-3.50	-2.96	-2.92	0.18	-0.39
5	[Mn(salen)SCN]	-3.80	-3.28	-3.24	0.22	0.24
6	[Mn(salen)Br]	-1.00	-0.72	-0.85	-0.12	0.32
7	[Mn(pterpy)Cl_3]	-3.53	-2.71	-2.87	0.23	-0.38

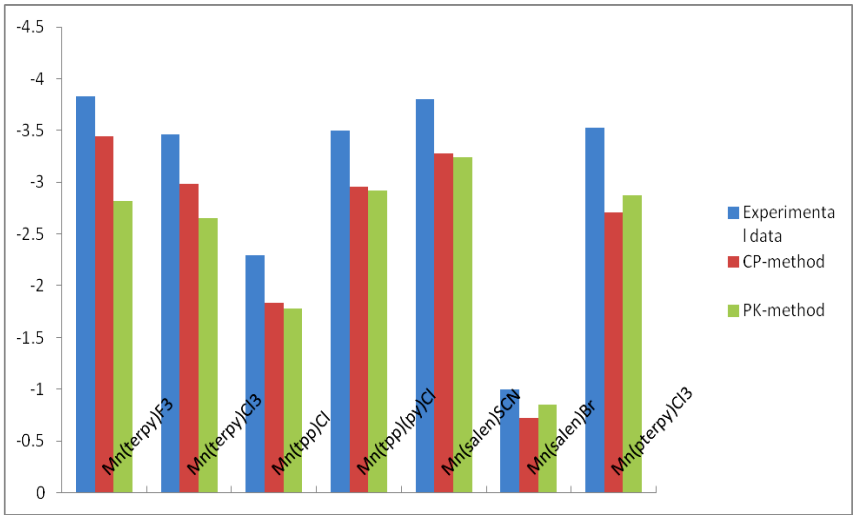

Figure 2.3: Comparative values for the experimental, the CP and the PK method

We observe that all the complexes exhibit negative D-values with finite uniaxial anisotropy. The negative D values signify that these complexes exhibit an axial elongated Jahn-Teller distortion which is typical in cases of d^4 high-spin configurations. As stated earlier the D_{SOC} part is being calculated using two approaches, viz. CP-SOC (coupled perturbed) and PK-SOC (Pederson-Khanna) methods. In almost all the cases

except in [Mn(salen)Br] and [Mn(pterpy)Cl_3] the CP approach gives value closer to the D_{Tot} experimental results while in these two abovementioned complexes the PK approach gives closer D-tensor values than the CP method.

Relative merits of both the CP and the PK methods are judged by linear regression curve obtained by plotting the experimental vs the calculated results. Also the standard error calculated therewith quantitatively explains the correlation between the experimental and theoretical results. We know that in symmetric environment both the experimental and theoretical D values are zero hence in linear regression we have forced the intercept to be zero. Table 2.5 gives the correlation coefficients and the standard error for both the SOC approaches.

Table 2.5: Comparison of CP and PK approach for the estimation of D-tensor

Method	**Correlation coefficient**	**Slope**	**Standard error**
CP-SOC	0.973	0.843	0.245
PK-SOC	0.967	0.799	0.305

Comparison of the two methods reveals that CP-SOC method yields D_{Tot} values much closer to the experimental value; the superiority of the CP-SOC approach over PK-SOC is in consistent with the previously published calculations as given in the above-mentioned references. This is attributed to the rigorously derived spin-flip terms in CP method.

Out of the two contributions towards D_{Tot}, D_{SS} accounts for 30% of the total D_{Tot} and the remaining contribution being from D_{SOC}. Thus D_{SS} has appreciable contribution which is attributed to the inclusion of spin-density of the complexes in D_{SS}.

The D_{SOC} part can be considered to decompose into four types of excitations [21]. Table 2.6 sums up all the decomposed SOC parts into various types of excitations.

Table 2.6: Various decomposed D-tensor values from the CP-SOC approach

Sl. No.	Complexes	D_{SOC}	α→α	β→β	α→β	β→β	D_{SS}	1-centre	2-centre	3-centre	4-centre
1	[Mn(terpy)F_3]	-2.31	-0.32	-0.58	-1.46	0.06	-1.13	-1.35	0.09	0.13	0.00
2	[Mn(terpy)Cl_3]	-2.19	-0.23	-0.79	-1.38	0.22	-0.79	1.16	-1.43	-0.47	-0.04
3	[Mn(tpp)Cl]	-1.29	0.06	-0.36	-1.20	0.19	-0.53	-0.50	-0.02	0.01	-0.05
4	[Mn(tpp)(py)Cl]	-2.15	-0.12	-0.56	-1.62	0.15	-0.80	-0.76	0.01	-0.04	0.00
5	[Mn(salen)SCN]	-2.59	0.55	-0.84	-2.23	-0.06	-0.69	-0.66	0.01	-0.04	0.00
6	[Mn(salen)Br]	-0.50	0.09	-0.13	-0.48	0.02	-0.22	-0.20	-0.01	-0.00	0.00
7	[Mn(pterpy)Cl_3]	-2.02	-0.33	-0.75	-1.28	0.33	-0.68	-1.12	0.36	0.08	-0.00

They are same-spin or spin-flip excitations viz., (i) excitation of a spin-down (β) electron from doubly occupied MO (DOMO) to a SOMO which results in the same spin as that of the ground state S, (β→β), (ii) a spin-up electron (α) excited from a singly occupied MO (SOMO) to a virtual MO (VMO) which leads to states of the same spin S as that of the ground state (α→α), (iii) excitations between two SOMO which is a spin-flip excitation leading to states of S´=S-1 (α→β) and (iv) another spin-flip excitation being a 'shell-opening' transition from a DOMO to a VMO and giving rise to states of S´=S+1 (β→α). The magnitude of the α→β contribution is the highest among the four types of excitations. The α→β excitation is dominated by ligand-field quintet-triplet excited states. All other excitations are considered to be charge-transfer contributions in the ligand-filed sense since in Mn(III) there are usually neither MLCT nor LMCT within the visible spectral range. The β→β contribution is found to be the least. This reveals that a tenuous balance between d-d spin flip, LMCT, MLCT, etc. excited states contribute to the total D_{SOC} .

he D_{SS} values are decomposed to n-center contributions where n=1-4. In addition to the four types of SOC excitations Table 2.6 summarizes the 1-, 2-, 3, and 4-centre contributions of the SS part that account to appreciable contribution of the spin-spin interaction towards D_{Tot}. ORCA decomposes D_{SS} values into four center contributions further as 1-centre, 2-centre Coulomb, 2-centre exchange, 2-centre hybrid, 3-centre exchange and 4-centre. The major contribution comes from the 1-centre term. We have also studied the HOMO-LUMO gap but no firm correlation between the same and D_{Tot} values can be derived. It may be so because the interpretation of the virtual orbital energies is absolutely different as soon as nonlocal HF exchange is mixed into a density functional as done in the case with hybrid DFT methods. Finally we can conclude that the DFT calculated g-tensor value ranges from 1.9-2.0 and therefore Mn(III) complexes have shown very little Zeeman anisotropy. We have done a comparative study of the two SOC approaches viz., CP (coupled-perturbed) and PK (Pederson-Khanna) methods to estimate D_{SOC} that would lead to closer experimental D-tensor values. The CP-SOC results proved to be in better agreement with the experimentally derived values. Also, with the ORCA program package we could split the total D_{SOC} values to spin-spin and spin-flip excitations.

REFERENCES

[1] Renault, J. P., Verchère−Béaur, C., Morgenstern−Badarau, I., Yamakura, F. and Gerloch, M. EPR and ligand field studies of iron superoxide dismutases and iron-substituted manganese superoxide dismutases: relationships between electronic structure of the active site and activity. *Inorganic Chemistry*, 39(12):2666−2675, 2000.

[2] Zhang, W., Loebach, J. L., Wilson, S. R. and Jacobsen, E. N. Enantioselective epoxidation of unfunctionalized olefins catalyzed by salen manganese complexes. *Journal of the American Chemical Society*, 112(7):2801−2803, 1990.

[3] Wilce, M. C. J., Bond, C. S., Dixon, N. E., Freeman, H. C., Guss, J. M., Lilley, P. E. and Wilce, J. A. Structure and mechanism of a proline-specific aminopeptidase from Escherichia coli. *Proceedings of the National Academy of Sciences,* volume 95(7), pages 3472−347. 1998.

[4] Bewley, M. C., Jeffrey, P. D., Patchett, M. L., Kanyo, Z. F. and Baker, E. N. Crystal structures of Bacillus caldovelox arginase in complex with substrate and inhibitors reveal new insights into activation, inhibition and catalysis in the arginase superfamily. *Structure,* 7:435−448, 1999.

[5] Yano, J., Kern, J., Sauer, K., Latimer, M. J., Pushkar, Y., Biesiadka, J. and Yachandra, V. K. Where water is oxidized to dioxygen: Structure of the photosynthetic Mn_4Ca cluster. *Science*, 314(5800):821−825, 2006.

[6] Barynin, V. V., Whittaker, M. M., Antonyuk, S. V., Lamzin, V. S., Harrison, P. M., Artymiuk, P. J. and Whittaker, J. W. Crystal structure of manganese catalase from Lactobacillus plantarum. *Structure*, 9(8):725−738, 2001.

[7] Katsuki, T. Catalytic asymmetric oxidations using optically active (salen) manganese (III) complexes as catalysts. *Coordination Chemistry Reviews*, 140:189−214, 1995.

[8] Palucki, M., Hanson, P. and Jacobsen, E. N. Asymmetric oxidation of sulfides with H_2O_2 catalyzed by (salen) Mn (III) complexes. *Tetrahedron Letters*, 33(47):7111−7114, 1992.

[9] Christou, G., Gatteschi, D., Hendrickson, D. N. and Sessoli, R. Single-molecule magnets. *Mrs Bulletin*, 25(11):66−71, 2000.

[10] Ritter, S. K. Single-molecule magnets evolve. *Chemical And Engineering News*, 82(50):29−32, 2004.

[11] Caneschi, A., Gatteschi, D., Lalioti, N., Sangregorio, C., Sessoli, R., Venturi, G. and Novak, M. A. Cobalt(II) nitronyl nitroxide chains as molecular magnetic nanowires. *Angewandte Chemie International Edition*, 40(9):1760−1763, 2001.

[12] Clérac, R., Miyasaka, H., Yamashita, M. and Coulon, C. Evidence for single-chain magnet behavior in a Mn^{III}-Ni^{II} chain designed with high spin magnetic units: a route to high temperature metastable magnets. *Journal of the American Chemical Society*, 124(43):12837−12844, 2002

[13] Liu, J., Qu, M., Rouzières, M., Zhang, X. M. and Clérac, R. A single-chain magnet based on $\{Co^{II}_4\}$ complexes and azido/picolinate ligands. *Inorganic chemistry*, 53(15):7870−7875, 2014.

[14] Cirera, J., Ruiz, E., Alvarez, S., Neese, F. and Kortus, J. How to build molecules with large magnetic anisotropy. *Chemistry-A European Journal*, 15(16):4078−4087, 2009.

[15] Chen, L., Wang, J., Liu, Y. Z., Song, Y., Chen, X. T., Zhang, Y. Q. and Xue, Z. L. Slow magnetic relaxation in mononuclear octahedral manganese (III) complexes with dibenzoylmethanide ligands. *European Journal of Inorganic Chemistry*, 2015(2):271−278, 2015.

[16] Kennedy, B. J. and Murray, K. S. Magnetic properties and zero-field splitting in high-spin manganese (III) complexes. 1. Mononuclear and polynuclear Schiff-base chelates. *Inorganic Chemistry*, 24(10):1552−1557, 1985.

[17] Ballhausen, C. J. *Introduction To Ligand Field Theory*. Mc-Graw Hill Ed. 1962.

[18] Lushington, G. H. and Grein, F. Complete to second-order ab initio level calculations of electronic g-tensors. *Theoretica Chimica Acta*, 93(5):259−267, 1996.

[19] Schreckenbach, G. and Ziegler, T. Calculation of the g-tensor of electron paramagnetic resonance spectroscopy using gauge-including atomic orbitals and

density functional theory. *The Journal of Physical Chemistry A*, 101(18):3388−3399, 1997.

[20] van Lenthe, E., Wormer, P. E. and van der Avoird, A. D. Density functional calculations of molecular g-tensors in the zero-order regular approximation for relativistic effects. *The Journal of Chemical Physics*, 107(7):2488−2498, 1997.

[21] Lushington, G. H. and Grein, F. Multireference configuration interaction calculations of electronic g-tensors for NO_2, H_2O^+, and CO^+. *The Journal of Chemical Physics*, 106(8):3292−3300, 1997.

[22] Ziegler, T. The 1994 Alcan Award Lecture Density functional theory as a practical tool in studies of organometallic energetics and kinetics. Beating the heavy metal blues with DFT. *Canadian Journal of Chemistry*, 73(6):743−761, 1995.

[23] Boča, R. Zero-field splitting in metal complexes. *Coordination Chemistry Reviews*, 248(9−10):757−815, 2004.

[24] Zein, S. and Neese, F. Ab initio and coupled-perturbed density functional theory estimation of zero-field splittings in MnII transition metal complexes. *The Journal of Physical Chemistry A*, 112(34):7976−7983, 2008.

[25] Neese, F. Importance of direct spin- spin coupling and spin-flip excitations for the zero-field splittings of transition metal complexes: a case study. *Journal of the American Chemical Society*, 128(31):0213−10222, 2006.

[26] Bruna, P. J., Lushington, G. H. and Grein, F. Stability, properties and electronic g-tensors of H_2CO^- as stabilized in H_2CONa complexes. *Chemical Physics*, 225(1−3):1−15, 1997.

[27] Neese, F. Prediction of electron paramagnetic resonance g values using coupled perturbed Hartree-Fock and Kohn-Sham theory. *The Journal of Chemical Physics*, 115(24):11080−11096, 2001.

[28] Kaupp, M., Reviakine, R., Malkina, O. L., Arbuznikov, A., Schimmelpfennig, B. and Malkin, V. G. Calculation of electronic g-tensors for transition metal complexes using hybrid density functionals and atomic meanfield spin-orbit operators. *Journal of Computational Chemistry*, 23(8):794−803, 2002.

[29] Sinnecker, S. and Neese, F. Spin-spin contributions to the zero-field splitting tensor in organic triplets, carbenes and biradicals a density functional and ab initio study. *The Journal of Physical Chemistry A*, 110(44):12267−12275, 2006.

[30] Neese, F. and Solomon, E. I. Calculation of zero-field splittings, g-values, and the relativistic nephelauxetic effect in transition metal complexes. Application to high-spin ferric complexes. *Inorganic Chemistry*, 37(26):6568−6582, 1998.

[31] Retegan, M., Collomb, M. N., Neese, F. and Duboc, C. A combined high-field EPR and quantum chemical study on a weakly ferromagnetically coupled dinuclear Mn (III) complex. A complete analysis of the EPR spectrum beyond the strong coupling limit. *Physical Chemistry Chemical Physics*, 15(1):223−2304, 2013.

[32] Neese, F. Calculation of the zero-field splitting tensor on the basis of hybrid density functional and Hartree-Fock theory. *The Journal of Chemical Physics*, 127(16):164112, 2007.

[33] McWeeny, R. On the origin of spin-Hamiltonian parameters. *The Journal Of Chemical Physics*, 42(5):1717−1725, 1965.

[34] Neese, F. *Orca*—an ab initio density functional, and semiempirical program package, version 2.9. University of Bonn, 2008.

[35] Duboc, C., Ganyushin, D., Sivalingam, K., Collomb, M. N. and Neese, F. Systematic theoretical study of the zero-field splitting in coordination complexes of Mn (III). Density functional theory versus multireference wave function approaches. *The Journal of Physical Chemistry A*, 114(39):10750−10758, 2010.

[36] Neese, F. Metal and ligand hyperfine couplings in transition metal complexes: The effect of spin–orbit coupling as studied by coupled perturbed Kohn–Sham theory. *The Journal of Chemical Physics*, 118(9):3939−3948, 2003.

[37] Ray, K., Begum, A., Weyhermüller, T., Piligkos, S., Van Slageren, J., Neese, F. and Wieghardt, K. The electronic structure of the isoelectronic, square-planar complexes $[Fe^{II}(L)_2]^{2-}$and $[Co^{III}(LBu)_2]^{-}$ (L_2−and $(LBu)_2$−= benzene−1,2−dithiolates): An experimental and density functional theoretical study. *Journal of the American Chemical Society*, 127(12):4403−4415, 2005.

[38] Schöneboom, J. C., Neese, F. and Thiel, W. Toward identification of the compound I reactive intermediate in cytochrome P450 chemistry: A QM/MM study of its EPR and Mössbauer parameters. *Journal of the American Chemical Society*, 127(16):5840−5853, 2005.

[39] Scheifele, Q., Riplinger, C., Neese, F., Weihe, H., Barra, A. L., Juranyi, F. and Tregenna−Piggott, P. L. Spectroscopic and theoretical study of a mononuclear manganese (III) complex exhibiting a tetragonally compressed geometry. *Inorganic Chemistry*, 47(2):439−447, 2008.

[40] Pantazis, D. A., Orio, M., Petrenko, T., Zein, S., Bill, E., Lubitz, W. and Neese, F. A new quantum chemical approach to the magnetic properties of oligonuclear transition-metal complexes: Application to a model for the tetranuclear manganese cluster of photosystem II. *Chemistry–A European Journal*, 15(20):5108−5123, 2009.

[41] Sinnecker, S., Neese, F., Noodleman, L. and Lubitz, W. Calculating the electron paramagnetic resonance parameters of exchange coupled transition metal complexes using broken symmetry density functional theory: Application to a Mn^{III}/Mn^{IV} model compound. *Journal of the American Chemical Society*, 126(8):2613−2622, 2004.

[42] Dutta, S. and Deka, R. C. Zero field splitting in Mn (III) complexes: A comparative study of DFT base Coupled-Perturbed and Pederson-Khanna approaches. *Computational and Theoretical Chemistry*, 1072:1−6, 2015.

[43] Becke, A. D. Density-functional exchange-energy approximation with correct asymptotic behavior. *Physical Review A*, 38(6):3098, 1988.

[44] Perdew, J. P. Density-functional approximation for the correlation energy of the inhomogeneous electron gas. *Physical Review B*, 33(12):8822, 1986.

[45] Schäfer, A., Huber, C., and Ahlrichs, R. Fully optimized contracted Gaussian basis sets of triple zeta valence quality for atoms Li to Kr. *The Journal of Chemical Physics*, 100(8):5829−5835, 1994.

[46] Weigend, F. Accurate Coulomb-fitting basis sets for H to Rn. *Physical Chemistry Chemical Physics*, 8(9):1057−1065, 2006.

[47] Heß, B. A., Marian, C. M., Wahlgren, U. and Gropen, O. A mean-field spin-orbit method applicable to correlated wavefunctions. *Chemical Physics Letters*, 251(5−6):365−371, 1996.

[48] Mantel, C., Chen, H., Crabtree, R. H., Brudvig, G. W., Pécaut, J., Collomb, M. N. and Duboc, C. High-spin chloro mononuclear MnIII complexes: A multifrequency high-field EPR study. *Chemphyschem*, 6(3):541−546, 2005.

[49] Mantel, C., Hassan, A. K., Pécaut, J., Deronzier, A., Collomb, M. N. and Duboc-Toia, C. A high-frequency and high-field EPR study of new azide and fluoride mononuclear Mn (III) complexes. *Journal of the American Chemical Society*, 125(40):12337−12344, 2003.

[50] Krzystek, J., Telser, T., Pardi, L. A., Goldberg, D. P., Hoffman, B. M. and Brunel, L. C. High-frequency and -field electron paramagnetic resonance of high-spin manganese(III) in porphyrinic complexes, *Inorganic Chemistry*, 38:6121–6129, 1999

[51] Behere, D. V. and Mitra, S. Magnetic susceptibility study and ground-state zero-field splitting in manganese (III) porphyrins. *Inorganic Chemistry*, 19(4):992−995, 1980.

[52] Kennedy, B. J. and Murray, K. S. Magnetic properties and zero-field splitting in high-spin manganese (III) complexes. 1. Mononuclear and polynuclear Schiff-base chelates. *Inorganic Chemistry*, 24(10):1552−1557, 1985